NANO LETTERS

Single-Element Diffraction-Limited Fisheye Metalens

Mikhail Y. Shalaginov,* Sensong An, Fan Yang, Peter Su, Dominika Lyzwa, Anuradha M. Agarwal, Hualiang Zhang, Juejun Hu,* and Tian Gu*

Cite This: *Nano Lett.* 2020, 20, 7429–7437

Read Online

ACCESS | Metrics & More | Article Recommendations | Supporting Information

ABSTRACT: Wide field-of-view (FOV) optical functionality is crucial for implementation of advanced imaging and image projection devices. Conventionally, wide FOV operation is attained with complicated assembly of multiple optical elements known as "fisheye lenses". Here we present a novel metalens design capable of performing diffraction-limited focusing and imaging over an unprecedented near 180° angular FOV. The lens is monolithically integrated on a one-piece flat substrate and involves only a single layer of metasurface that corrects third-order Seidel aberrations including coma, astigmatism, and field curvature. The metalens further features a planar focal surface, which enables considerably simplified system architectures for applications in imaging and projection. We fabricated the metalens using Huygens meta-atoms operating at 5.2 μm wavelength and experimentally demonstrated aberration-free focusing and imaging over the entire FOV. The design concept is generic and can be readily adapted to different meta-atom geometries and wavelength ranges to meet diverse application demands.

KEYWORDS: Metalens, wide field of view, Huygens metasurface, diffraction-limited focusing
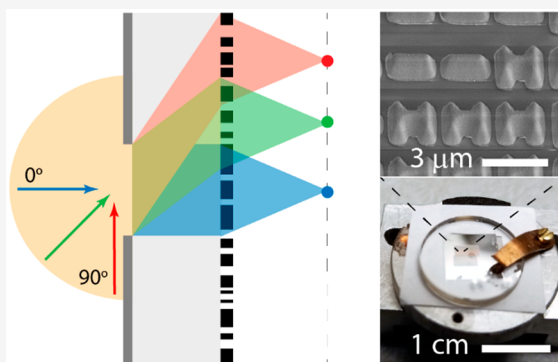
Optical systems with large FOV are vital to high performance imaging, detection, image or beam projection, and Fourier optics.[1−4] One of the earliest examples of such systems is the panoramic camera pioneered by Thomas Sutton in the year 1858, which consisted of a single water-filled spherical lens producing an image on a curved glass plate covered with reactive emulsion. Because of apparent difficulties in fabrication and handling of curved plates, the original approach was soon abandoned, but it outlines the fundamental challenges associated with achieving wide-FOV imaging. Since then, panoramic photography has been evolving along the path of planar detector planes while relying on compound lens assemblies, commonly known as "fisheye lenses", to reduce optical aberrations at large field angles. Such multilens architecture, however, increases the size, weight, and assembly complexity of optical systems.

Metasurfaces, devices capable of controlling the phase, amplitude and polarization of light with arrays of subwavelength structures, present a promising solution enabling flat and compact optical components.[5−14] Metasurface-based designs have been widely employed for constructing planar ultrathin lenses, also called metalenses,[15−22] to mitigate several types of aberrations,[23] in particular, spherical[16] and chromatic[24−27] aberrations. However, angle-dependent aberrations (e.g., coma, astigmatism, and field curvature) are among the major challenges that must be overcome to realize optical systems with enhanced functionalities while maintaining a minimum element count.[28,29]

Phase profile variation due to different angles of incidence (AOIs) results in third-order (Seidel) aberrations such as coma, astigmatism, and field curvature, which limit the FOV. As an example (see Supporting Information), assuming a baseline metalens design with 1 mm diameter and 2 mm focal length operating at a wavelength of 5.2 μm, the conventional hyperbolic phase profile only allows diffraction-limited focusing at AOIs up to 7°, beyond which coma becomes the dominant aberration and rapidly degrades the metalens imaging performance. The small viewing angle significantly limits the use of a single metalens in imaging and image projection applications.

Several metalens designs have already been implemented to suppress coma and expand the diffraction-limited FOV. One approach entails engraving metasurfaces on spherical surfaces; however, this poses a nontrivial fabrication challenge.[23] Another solution involves cascading multiple metasurfaces based on traditional bulk optical system design principles. In such doublet metalens designs,[28,29] the focusing function is primarily performed by one of the metasurfaces while the other

Table 1. Optical Metalenses with Diffraction-Limited Wide FOV Performance

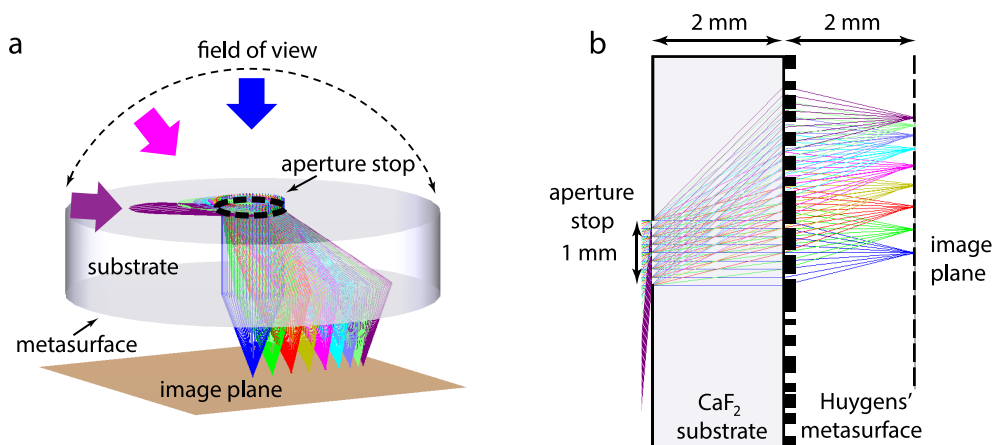|	diffraction-limited FOV (deg)	focusing efficiency (%)	number of metasurface layers	wavelength (nm)	numerical aperture
Arbabi et al.[28]	56	45−70	2	850	0.49
Groever et al.[29]	50	30−50	2	470−660	0.44
Engelberg et al.[30]	30	6−20	1	825	0.2
this work (mid-IR, experiment)	>170	32−45	1	5200	0.24
this work (near-IR, simulation)	≈ 180	41−88	1	940	0.2

Figure 1. Principle of operation. (a) Schematic of a single-layer planar metalens with an ultrawide FOV. (b) Side-view of an exemplary design based on mid-IR Huygens metasurface.

acts to correct the on-axis wavefront aberrations. Diffraction-limited FOV up to approximately 56° was demonstrated in such doublets.[28] In comparison, the FOV of a single-layer metalens has been limited to 30° with reduced diffraction limit resolution due to vignetting,[30] and the design further suffers from low optical efficiencies of 6−20% and sensitivity to assembly misalignment (Table 1). Metalenses with large FOV performance rivaling their traditional refractive counterparts have not been realized to date.

In this paper, we demonstrate the first panoramic metalens with a record-breaking diffraction-limited FOV exceeding 170°, which was originally reported in ref 31. The wide field-of-view (WFOV) metalens assumes a simple and easy-to-fabricate configuration, consisting of only a single metasurface layer and an aperture co-integrated on a single thin substrate. Moreover, the lens has a planar focal surface, which significantly simplifies the associated detector (for imaging and detection) or light emitter (for image/beam projection, display, etc.) array design. Here, we experimentally implemented the design in the mid-infrared (mid-IR) using Huygens meta-atoms,[32−40] although the design is completely generic and scalable to other meta-atom structures and wave bands. The metalens design concept, fabrication approach, and characterization results are described in the following sections.

Results. *Extreme Wide FOV Metalens: The Concept.* The basic concept of the WFOV metalens is schematically illustrated in Figure 1a. It consists of a single substrate with an input aperture positioned on the front surface and a metasurface positioned on the back surface. Light beams incident on the input aperture at different AOIs θ_i are refracted to the backside metasurface and then focused onto a planar focal plane.

Similar to a Chevalier landscape lens, our metalens design concept spatially decouples the metasurface and aperture stop but positions them on a common, planar substrate. Such an

optical architecture allows input beams at different AOIs to be captured on different yet continuous portions of the flat metasurface.[41] The planar aperture uniformly projects and angularly separates the beams without introducing additional wavefront distortion. When configured into an image-space telecentric lens, the chief rays in the image space are always perpendicular to the image plane. With the telecentric configuration, the desired local metasurface phase map for focusing light incident at an oblique AOI corresponds to the sum of a standard hyperbolic profile over the aperture and a linear phase gradient induced by the oblique incidence. While a rigorous solution does not exist for an ideal phase profile which perfectly meets the condition at all AOIs over a continuous FOV (Figure S9a), we can identify close approximations (Figure S9b) of the solution with minimal phase deviations from the ideal case via numerical optimization (detailed in the Discussion). The phase profile is designed so that the RMS wavefront error from an ideal spherical wavefront over the input aperture is always smaller than 0.07 wavelength for all AOIs. This, in theory, ensures that a Strehl ratio over 0.8 can be maintained over the entire field-of-view,[23] thereby achieving diffraction-limited performance in various light illumination conditions. In the Supporting Information, we also furnish an intuitive explanation justifying the exceptional WFOV performance of our design.

It is important to distinguish our approach from spatially multiplexed designs,[42,43] where nonoverlapping regions on a metasurface are dedicated to beams at different AOIs. As a result, such metalenses can only achieve high quality focusing for a discrete set of AOIs. In our case, the judiciously designed metasurface phase profile and metalens architecture allow diffraction-limited focusing of beams with continuously varying AOIs despite mutually overlapping beam profiles on the metasurface. Therefore, our metalens can achieve aberration-free beam focusing or conversely, beam collimation and, hence,
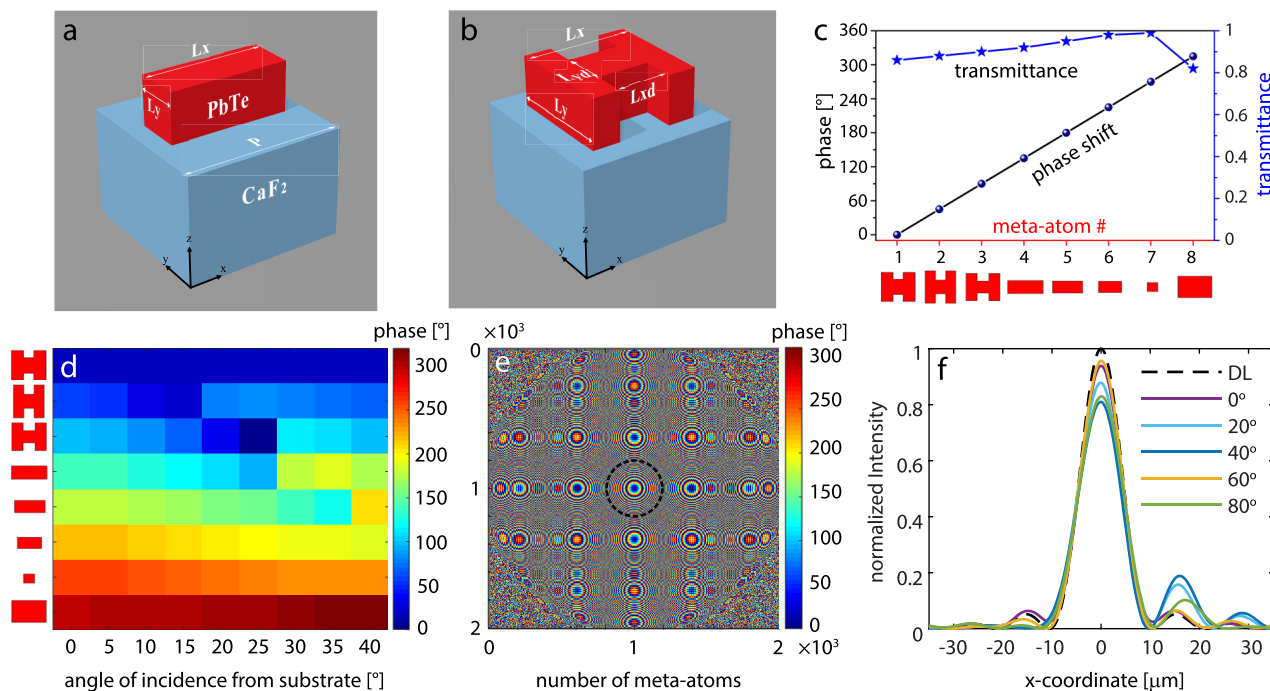
Figure 2. Metalens design. Tilted view of a (A) rectangular and an (B) H-shaped meta-atom. The thickness of the PbTe blocks is 650 nm, while the lattice constant is 2.5 μm along both x and y axes. (C) Transmittance and phase shift of the eight meta-atoms used to construct the metalens at normal incidence. Sketches of corresponding meta-atoms are listed beneath the plot. Detailed dimensions are listed in the Supporting Information. (D) Angle-dependent phase delay imparted by the meta-atoms, showing weak dependence to AOI. The angle of 45.6° concurs with the angle of total internal reflection at the interface between air and calcium fluoride. The incident light is TM-polarized. (E) Metalens phase distribution. Black dash-line circle indicates the front aperture position. (F) Simulated cross-sectional intensity distributions of focal spots under different AOIs and a focal spot formed by a perfect lens (DL: diffraction-limited) of the same NA.

image projection for any light direction from or to any point on the front hemisphere.

In addition to correcting aberrations such as coma and astigmatism, the metalens features a planar focal plane across the entire FOV. The elimination of Petzval field curvature presents a critical benefit to imaging and image projection applications by facilitating standard planar detector or emitter array integration.

A schematic of an exemplary WFOV metalens design operating at a wavelength of 5.2 μm is shown in Figure 1b. A 2-mm-thick calcium fluoride (CaF$_2$) planar substrate (n_{sub} = 1.4 at 5.2 μm) is used. A 1-mm-diameter circular aperture is positioned on the substrate front side, and a 5.2 × 5.2 mm^2 metasurface is patterned on the back side. The metasurface contains 2000 × 2000 Huygens meta-atoms made of PbTe with a square lattice constant of 2.5 μm. The metasurface is designed to have a constant focal length of 2 mm, corresponding to an effective numerical aperture (NA) of 0.24.

Device Design and Modeling. The metalens was designed utilizing a hierarchical combination of a finite element method (FEM) and Kirchhoff diffraction integral as described in Materials and Methods. The Huygens meta-atoms comprise rectangular or H-shaped blocks made of PbTe resting on a CaF$_2$ substrate (Figures 2a,b). This material combination features low optical losses and giant refractive index contrast in the mid-IR, enabling transmissive metasurfaces supporting both electric and magnetic dipole (ED and MD) resonances.[35] Designed to spectrally overlap ED and MD resonances at the operation wavelength, a full 2π phase coverage with near-unity transmittance can be potentially achieved, leveraging the Kerker effect.[36] The amplitude and phase responses of a

group of 8 meta-atoms simulated at normal incidence are illustrated in Figure 2c (Supporting Information, Table S3). The phase shift of each meta-atom at oblique AOIs (inside the substrate) was also simulated and summarized in Figure 2d. The results indicate that the meta-atom responses are only weakly dependent on AOIs (see Supporting Information for further details).

The metasurface optimization process involves iterative evaluation between OpticStudio (Zemax, LLC) and the Kirchhoff diffraction integral model on the focal spot quality, that is, Strehl ratio at different AOIs (SR$_{AOI(i)}$). The following merit function (figure of merit, FOM) is maximized using numerical optimization:

$$\text{FOM} = \sum_i w_{AOI(i)} \cdot SR_{AOI(i)} \qquad (1)$$

where $w_{AOI(i)}$ represents the weighting factors at different AOIs. This form of FOM simultaneously examines multiple beams over the entire FOV. The optimized metalens phase profile is shown in Figure 2e and further detailed in the Supporting Information. Compared to a perfect lens with the same NA, the designed phase profile leads to Strehl ratios better than 0.8 at all AOI values, therefore achieving diffraction limited focusing and imaging performance across the entire FOV (Figure 2f). Modulation transfer functions (MTF) simulated at different AOIs are shown in Figure S4 to further support this conclusion.

Metalens Fabrication and Characterization. The metalens was fabricated using electron beam lithography on a 2-mm-thick CaF$_2$ planar substrate by a double-resist-layer lift-off method following previously published protocols (see

Materials and Methods for full details).[35] Figure 3 shows an SEM top-view micrograph of the fabricated metasurface, confirming good pattern fidelity consistent with our design.
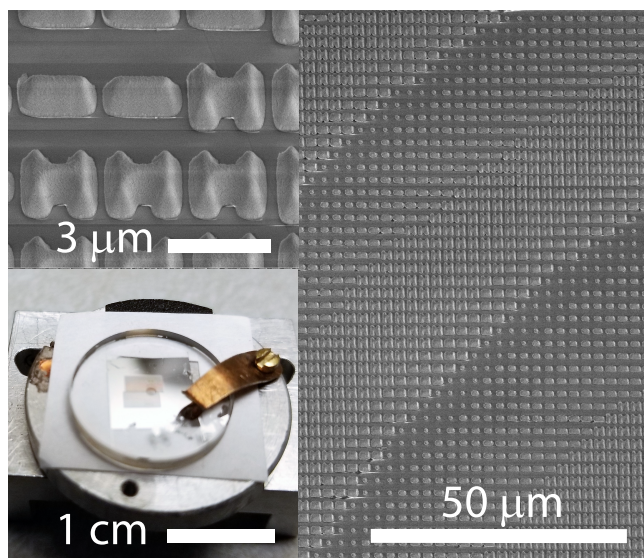

Figure 3. Fabricated metasurface. Photograph of the metalens sample and scanning electron microscopy (SEM) images of the meta-atoms.

We started with characterizing the focal spot quality of the lens at various AOIs. Several examples of the focal spot images are presented in Figures 4b−g, and the cross-sectional optical intensity profiles of the focal spots at 0°, 70°, and 85° AOIs are plotted in Figure 4h inset alongside the simulated ideal focal spot profiles from an aberration-free lens with the same NA for comparison. We further computed the Strehl ratios from the measurement following previously established procedures (Figure 4h).[35,44] For all the AOIs, the Strehl ratio remains above 0.8, indicating diffraction-limited focusing performance of the metalens.

We then quantified focusing efficiency of the lens, which is defined as the ratio between the power confined at the focal spot and the power incident onto the metasurface. Details of the measurement protocols are furnished in the Supporting Information. Figure 4i presents the measured focusing efficiency at different AOIs for linearly polarized light. The result indicates a relatively weak dependence on the AOIs varying from 45% to 32% as the angle of incidence changes from 0° to 85°. This relatively flat angular response is a useful feature in providing nearly uniform illumination across an image formed by the metalens.

Metalens Imaging Demonstration. To demonstrate the WFOV imaging capability, we used a setup depicted in Figure 4j, where the metalens collects the light scattered by an object and projects it onto the InSb FPA camera through a mid-IR lens. In the experiment, the distance between the object plane
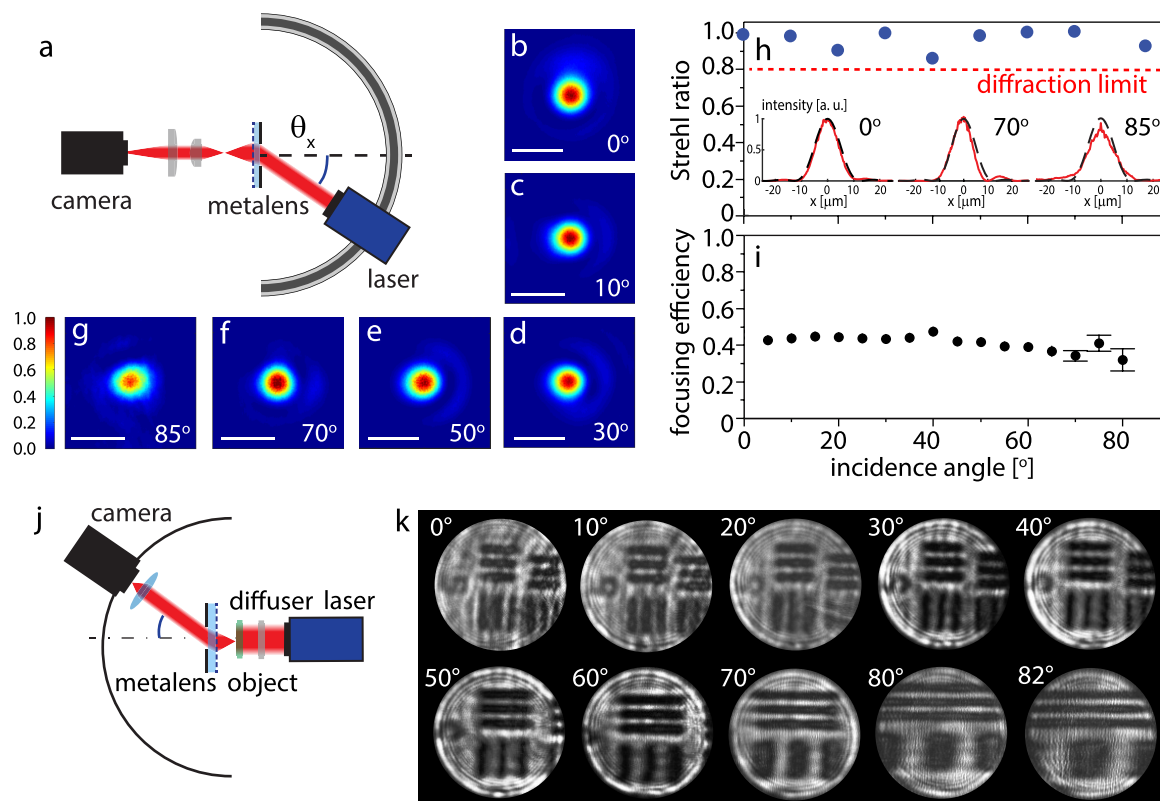

Figure 4. Metalens characterization and imaging demonstration. (a) Schematic of experimental setup for imaging a focal spot produced by metasurface at various AOIs. Examples of focal spot intensity images captured by FPA camera at (b) 0°, (c) 10°, (d) 30°, (e) 50°, (f) 70°, and (g) 85°. (h) Diffraction-limited focusing capability was concluded from the Strehl ratio values consistently above 0.8 threshold. Inset: focal spot cross sections at 0°, 70°, and 85° AOIs, measured data—solid red line, theoretical results for aberration-free lens with the same NA. (i) Metalens focusing efficiency was measured to be ~40% at all AOIs. (j) Schematic of imaging setup, where the object is illuminated by a laser beam. (k) Projected images of the 1951 USAF resolution test target with a period of 13.9 μm.
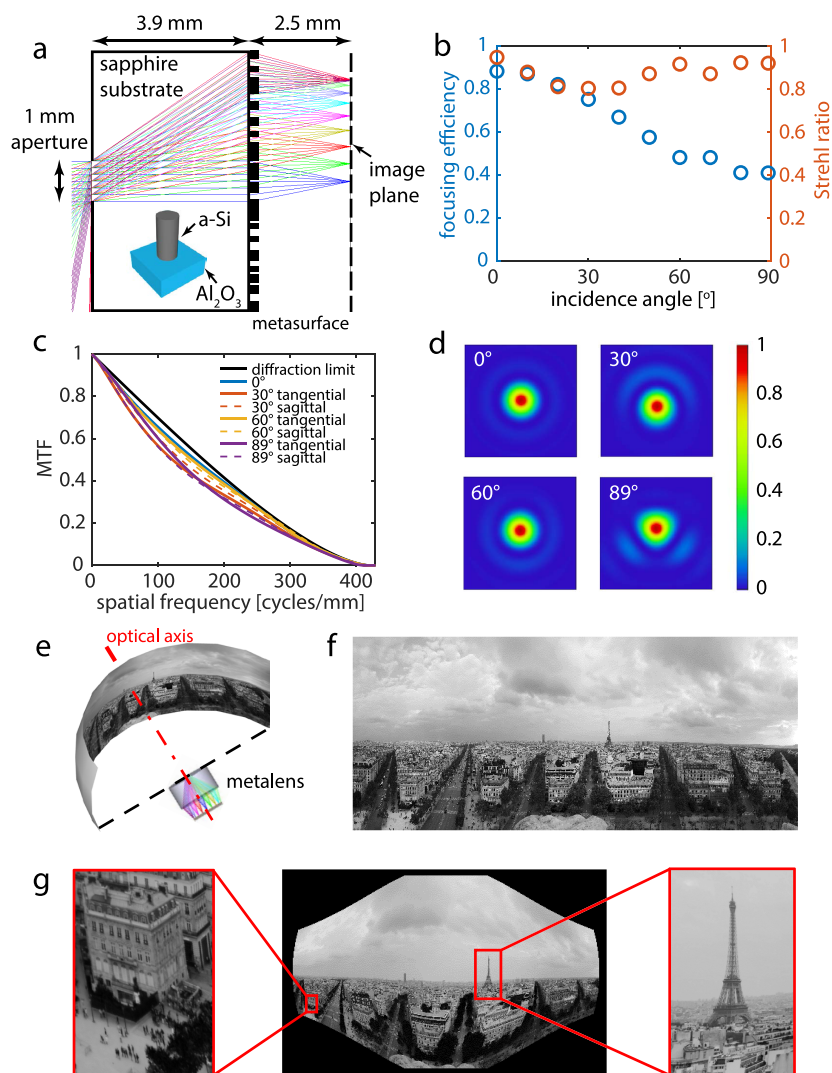
Figure 5. Simulations of exemplary WFOV metalens in NIR. (a) Side-view of an exemplary WFOV metalens design operating at 940 nm wavelength. Inset: meta-atom configuration. Simulated (b) Strehl ratio and focusing efficiency, (c) MTF, and (d) focal spots of the metalens at different AOIs. (e) Schematic of imaging simulation setup (not drawn to scale). (f) Monochromatic source image. (g) Simulated image formed by the metalens.

and the metalens is fixed to 2 mm to be consistent with the planar geometry of the metalens focal plane. The image at a specified angle was captured by moving the test target sideways (within the object plane) and adjusting the position of the camera. The object consists of metallic tin patterns replicating the USAF resolution test chart. The selected test target pattern (Group 5, Element 2) contains six stripes, each 13.9 μm wide, close to the ideal diffraction-limited resolution of the lens (13.2 μm). For comparison, we also performed simulation of the same imaging setup using OpticStudio, in which the metalens was replaced with a perfect aberration-free lens of the same numerical aperture. The simulated image shows excellent agreement with the experimental result (Figure S10). Figure 4k shows clearly resolved images of the pattern recorded at the full angular range of our experimental setup from 0° to 82° (the measurement range is similarly bound by geometric constraints of our experimental setup). We also note that while image distortion is apparent at AOIs larger than 60° (which is inevitable to all wide-FOV optical systems), such distortion does not compromise the image resolution, as indicated by previous PSF and MTF results. The result confirms diffraction-limited imaging performance of the metalens over a record wide angular regime.

Discussion. In our experiment, we have chosen to embody the WFOV design using a Huygens metasurface operating in the mid-IR. The implementation leverages our previously demonstrated a PbTe-on-CaF$_2$ meta-atom platform with established benefits including exceptionally high index contrast conducive to high-quality-factor Mie resonances, an ultrathin meta-atom profile, and ease of fabrication. The choice of a Huygens metasurface structure at the same time imposes constraints such as sensitivity to polarization and wavelength (our prior work has shown diffraction-limited performance across ~300 nm wavelengths in the mid-IR, corresponding to 6% fractional bandwidth[35]). We want to highlight that the wide-FOV design principle described herein is generic and applicable to arbitrary meta-atom configurations. Thus, with proper choice of meta-atoms, our design can also lead to panoramic metalenses with on-demand characteristics including broadband operation and polarization diversity. We note that certain limitations may apply on efficiency or NA when extending the design to broadband applications.[45] These are

important considerations to be accounted for when constructing wide-FOV achromatic metalenses. In addition, computational post-processing can be further utilized to enhance the performance of such designs.[46]

To showcase versatility of our approach, we present a polarization-insensitive near-infrared (NIR) metalens design with diffraction-limited performance covering an entire hemispherical view. Figure 5a illustrates an exemplary WFOV metalens design operating at 940 nm wavelength and with an effective NA of 0.2. The metasurface consists of amorphous Si (a-Si) nanoposts patterned on the back surface of a sapphire (Al_2O_3) substrate and an aperture stop positioned on the front side of the substrate. The nanopost diameters are changed to create varying phase delay covering 0 to 2π.[47−50] The metalens and metasurface designs are detailed in the Supporting Information.

As shown in Figure 5b, the simulated Strehl ratios are over 0.8 across the entire FOV, indicative of aberration-free focusing performance. The focusing efficiency of the metasurface versus AOIs (Figure 5b) closely follows the average transmittance response of the meta-atoms (Figure S7b), indicating minimal phase errors induced at both the meta-atom and metasurface levels.

Imaging performance of the NIR WFOV metalens is numerically investigated using OpticStudio. Figure 5c and d plot the MTF and focal spot intensities of the metalens simulated at different AOIs. Our WFOV metasurface design achieves a diffraction-limited spatial resolution of 2.9 μm on the image plane and an average angular resolution of approximately 0.1° across the entire 180 °FOV. To evaluate its imaging performance, we further used a monochromatized, stitched 180° horizontal panoramic photo of Paris taken from the Arc de Triomphe de l'Étoile[51] (Figure 5f) as the scene that is positioned an infinite distance away from the metalens. Figure 5e and g show the imaging configuration and captured image, respectively (more details in the Supporting Information). Despite the apparent barrel distortion, which is inherent to all wide-angle optical systems, the WFOV metalens can readily image the scene from all angles with high quality and minimal aberrations. The distortion can be straightforwardly corrected with post-processing, and the angular resolution can be further improved by increasing the aperture size while keeping the same NA. This design example reinforces that our WFOV design concept is generic and can be readily adapted to different meta-atom geometries and wavelength ranges to meet diverse application demands.

Conclusions. We proposed and demonstrated a novel metalens architecture and design to enable ultrawide-angle panoramic imaging and image projection. Our approach uniquely combines an unprecedented hemispherical FOV, diffraction-limited performance over the entire FOV, a remarkably compact and simple configuration involving only one metasurface layer on a flat substrate, and a planar focal plane ideal for optical system integration. As a proof-of-concept, we validated the design in the mid-IR wave band using Huygens metasurfaces, experimentally realizing a metalens with a record diffraction-limited FOV exceeding 170°. The same meta-optic architecture can be readily adapted to other wavelength ranges and meta-atom platforms. These critical advantages foresee potential integration of the technology in next-generation systems for imaging, optical projection, augmented reality/virtual reality, beam steering, and 3-D depth sensing applications.

Materials and Methods. *Metasurface Fabrication.* The sample was fabricated on a circular CaF_2 substrate (Edmund Optics) with a diameter of 15 mm and a thickness of 2 mm. Given inherent symmetry of the metasurface layout, only a 2 mm × 3.6 mm section of the metasurface was needed and fabricated to validate the WFOV performance. Prior to fabrication, the substrate surface was cleaned in sequential acetone and isopropanol alcohol (IPA) sonication baths for 3 min each. Afterward, the sample was baked at 190 °C for 5 min to fully evaporate the solvent and adsorbed moisture on its surface. Then the substrate was treated with oxygen plasma (150 W, 1 min, pressure 0.8 Torr) to remove organic residue contaminants. One side of the sample was covered with a double-layer photoresist composed of PMGI (800 nm thick) and ZEP 520A (400 nm thick). The PMGI layer was spin-coated at 2400 rpm (rpm) for 1 min, then baked at 190 °C for 3 min. The baking step is critical for assuring mechanical stability of the PMGI layer. The ZEP layer was spin-coated at 4000 rpm for 1 min and baked at 190 °C for 2 min. To prevent charging effects while performing electron beam (e-beam) lithography, we covered the sample with a water-soluble conductive polymer (ESpacer 300Z, Showa Denko America, Inc.) and placed a conducting clamp on top of the substrate.[52] The metasurface patterns were written with an e-beam lithography system (Elionix ELS F-125) at a voltage of 125 kV, current 10 nA, and proximity effect correction (PEC) with a base dose of 380 μC/cm^2. The ZEP layer was developed by submerging the sample into water, ZEDN50, and IPA for 1 min each. The PMGI layer was subsequently partially dissolved with RD6 developer diluted in a 1:1 ratio with water. This step must be done carefully to achieve a necessary undercut and not to collapse the pattern. After photoresist development, a 650 nm-thick PbTe film was deposited by thermal evaporation in a custom-designed system (PVD Products, Inc.) at a rate of 17 Å/s and a base pressure of 10^{-6} Torr.[53,54] Before deposition, the sample was precleaned with oxygen plasma to improve adhesion of the film. Later the metasurface pattern was transferred by lifting off the material on top of the photoresist by overnight soaking in *N*-methyl-2-pyrrolidone (NMP). On the other side of the sample, we patterned a circular aperture of 1 mm in diameter. The side patterned with the PbTe metasurface was protected by a dry film photoresist (DuPont MX5000 series) during the aperture fabrication. To fabricate the aperture, the surface was cleaned with oxygen plasma and spin-coated with a negative photoresist NR9−1000PY (Futurrex, Inc.) at 1500 rpm for 1 min. The sample was soft baked at 115 °C, exposed to UV light through the mask for 40 s (Karl Suss MA6Mask Aligner), and hard-baked at 155 °C. The exposed photoresist was subsequently developed in the aqueous developer RD6 (Futurrex, Inc.) for 10 s and rinsed with deionized water afterward. Then a 200 nm layer of metal tin was deposited by thermal evaporation and lifted off by removing the photoresist with acetone. Finally, the dry film photoresist covering the metasurface side was removed by overnight NMP treatment.

Device Modeling. The metalens was designed and modeled using a hierarchical combination of full-wave and Kirchhoff diffraction integral. At the subwavelength-scale, full wave FEM simulations were implemented to design and model the meta-atoms for desired optical responses. At the macroscopic system level, the diffraction integral method incorporating the full wave simulation results enables computationally efficient validation of the focusing characteristics of the entire metalens

and was used to optimize the phase profile of the metasurface (see Supporting Information for further details).

The meta-atom simulations were carried out with a frequency domain solver in the commercial software package CST Microwave Studio. For each meta-atom, unit cell boundary conditions were employed at both negative and positive x and y directions, while open boundary conditions were set along the z-axis. Each meta-atom was illuminated from the substrate side with an x-polarized plane wave pointing toward the positive z direction. The results shown in Figure 2c are the phase and amplitude of the complex transmission coefficient derived between the two open ports placed at the top and bottom of each meta-atom.

The initial optical structure and phase profile are designed using OpticStudio (Zemax, LLC). An analytical model based on the Kirchhoff diffraction integral is subsequently utilized to analyze the full metasurface performance under different AOIs. The model incorporates angular-dependent phase masks following individual meta-atom responses under different AOIs obtained from full wave simulations (Supporting Information, Figure S3). The Kirchhoff diffraction integral is a physically rigorous form of the Huygens-Fresnel principle.[55] The model starts with computing the Huygens point spread function of the optical system. It incorporates angular-dependent phase profiles at the metasurface and propagates wavefronts emitted from each meta-atom with corresponding amplitude and phase to the image plane where its complex amplitude is derived. The diffraction of the wavefront through space is given by the interference or coherent sum of the wavefronts from the Huygens sources. The intensity at each point on the image plane is the square of the resulting complex amplitude sum.

■ ASSOCIATED CONTENT

Ⓢ Supporting Information

The Supporting Information is available free of charge at https://pubs.acs.org/doi/10.1021/acs.nanolett.0c02783.

> Baseline metalens design using standard hyperbolic phase profile; design of WFOV metalens; efficiency measurements; NIR WFOV metalens design; NIR WFOV metalens image simulation; intuitive explanation of WFOV performance; imaging with mid-IR WFOV metalens (PDF)

■ AUTHOR INFORMATION

Corresponding Authors

Mikhail Y. Shalaginov − *Department of Materials Science & Engineering, Massachusetts Institute of Technology, Cambridge, Massachusetts 02139, United States;* Ⓞ orcid.org/0000-0002-1251-7766; Email: mys@mit.edu

Juejun Hu − *Department of Materials Science & Engineering and Materials Research Laboratory, Massachusetts Institute of Technology, Cambridge, Massachusetts 02139, United States;* Email: hujuejun@mit.edu

Tian Gu − *Department of Materials Science & Engineering and Materials Research Laboratory, Massachusetts Institute of Technology, Cambridge, Massachusetts 02139, United States;* Ⓞ orcid.org/0000-0003-3989-6927; Email: gutian@mit.edu

Authors

Sensong An − *Department of Electrical & Computer Engineering, University of Massachusetts Lowell, Lowell,*
Massachusetts 01854, United States; Ⓞ orcid.org/0000-0003-4098-916X

Fan Yang − *Department of Materials Science & Engineering, Massachusetts Institute of Technology, Cambridge, Massachusetts 02139, United States*

Peter Su − *Department of Materials Science & Engineering, Massachusetts Institute of Technology, Cambridge, Massachusetts 02139, United States*

Dominika Lyzwa − *Department of Biological Engineering, Massachusetts Institute of Technology, Cambridge, Massachusetts 02139, United States*

Anuradha M. Agarwal − *Department of Materials Science & Engineering and Materials Research Laboratory, Massachusetts Institute of Technology, Cambridge, Massachusetts 02139, United States*

Hualiang Zhang − *Department of Electrical & Computer Engineering, University of Massachusetts Lowell, Lowell, Massachusetts 01854, United States*

Complete contact information is available at:
https://pubs.acs.org/10.1021/acs.nanolett.0c02783

Author Contributions

T.G. conceived the metalens concept. M.Y.S. fabricated the devices. T.G. and S.A. designed and modeled the devices. M.Y.S. and T.G. performed device characterizations. T.G., M.Y.S., and S.A. analyzed the experimental data. P.S. contributed to device fabrication. F.Y. and D.L. contributed to optical testing. M.Y.S., T.G., and J.H. drafted the manuscript. J.H., T.G., H.Z., and A.A. supervised and coordinated the research. All authors contributed to revising the manuscript and technical discussions.

Notes

The authors declare no competing financial interest.

■ ACKNOWLEDGMENTS

■ REFERENCES

(1) Liu, W.; Li, Z.; Cheng, H.; Tang, C.; Li, J.; Zhang, S.; Chen, S.; Tian, J. Metasurface Enabled Wide-Angle Fourier Lens. *Adv. Mater.* **2018**, *30* (23), 1706368.

(2) Jiang, Z. H.; Lin, L.; Ma, D.; Yun, S.; Werner, D. H.; Liu, Z.; Mayer, T. S. Broadband and Wide Field-of-View Plasmonic Metasurface-Enabled Waveplates. *Sci. Rep.* **2015**, *4*, 7511.

(3) Lee, G. Y.; Hong, J. Y.; Hwang, S. H.; Moon, S.; Kang, H.; Jeon, S.; Kim, H.; Jeong, J. H.; Lee, B. Metasurface Eyepiece for Augmented Reality. *Nat. Commun.* **2018**, *9* (1), 4562.

(4) Guo, Y.; Ma, X.; Pu, M.; Li, X.; Zhao, Z.; Luo, X. High-Efficiency and Wide-Angle Beam Steering Based on Catenary Optical Fields in Ultrathin Metalens. *Adv. Opt. Mater.* **2018**, *6* (19), 1−8.

(5) Yu, N.; Tetienne, J.-P.; Aieta, F.; Kats, M. A.; Capasso, F.; Genevet, P.; Yu, N.; Gaburro, Z. Light Propagation with Phase Discontinuities: Generalized Laws of Reflection and Refraction. *Science* **2011**, *334* (6054), 333−337.

(6) Ni, X.; Emani, N. K.; Kildishev, A. V.; Boltasseva, A.; Shalaev, V. M. Broadband Light Bending with Plasmonic Nanoantennas. *Science* **2012**, *335* (6067), 427−427a.

(7) Pors, A.; Bozhevolnyi, S. I. Efficient and Broadband Quarter-Wave Plates by Gap-Plasmon Resonators. *Opt. Express* **2013**, *21* (3), 2942.

(8) Kuznetsov, A. I.; Miroshnichenko, A. E.; Brongersma, M. L.; Kivshar, Y. S.; Luk'yanchuk, B. Optically Resonant Dielectric Nanostructures. *Science* **2016**, *354* (6314), aag2472.

(9) Capasso, F. The Future and Promise of Flat Optics: A Personal Perspective. *Nanophotonics* **2018**, *7* (6), 953−957.

(10) Achouri, K.; Caloz, C. Design, Concepts, and Applications of Electromagnetic Metasurfaces. *Nanophotonics* **2018**, *7* (6), 1095−1116.

(11) Kamali, S. M.; Arbabi, E.; Arbabi, A.; Faraon, A. A Review of Dielectric Optical Metasurfaces for Wavefront Control. *Nanophotonics* **2018**, *7*, 1041−1068.

(12) Campbell, S. D.; Sell, D.; Jenkins, R. P.; Whiting, E. B.; Fan, J. A.; Werner, D. H. Review of Numerical Optimization Techniques for Meta-Device Design [Invited]. *Opt. Mater. Express* **2019**, *9* (4), 1842.

(13) Shaltout, A. M.; Lagoudakis, K. G.; van de Groep, J.; Kim, S. J.; Vučković, J.; Shalaev, V. M.; Brongersma, M. L. Spatiotemporal Light Control with Frequency-Gradient Metasurfaces. *Science* **2019**, *365* (6451), 374−377.

(14) Das Gupta, T.; Martin-Monier, L.; Yan, W.; Le Bris, A.; Nguyen-Dang, T.; Page, A. G.; Ho, K. T.; Yesilköy, F.; Altug, H.; Qu, Y.; Sorin, F. Self-Assembly of Nanostructured Glass Metasurfaces via Templated Fluid Instabilities. *Nat. Nanotechnol.* **2019**, *14*, 320−327.

(15) Shi, H.; Wang, C.; Du, C.; Luo, X.; Dong, X.; Gao, H. Beam Manipulating by Metallic Nano-Slits with Variant Widths. *Opt. Express* **2005**, *13* (18), 6815.

(16) Aieta, F.; Genevet, P.; Kats, M. A.; Yu, N.; Blanchard, R.; Gaburro, Z.; Capasso, F. Aberration-Free Ultrathin Flat Lenses and Axicons at Telecom Wavelengths Based on Plasmonic Metasurfaces. *Nano Lett.* **2012**, *12* (9), 4932−4936.

(17) West, P. R.; Stewart, J. L.; Kildishev, A. V.; Shalaev, V. M.; Shkunov, V. V.; Strohkendl, F.; Zakharenkov, Y. A.; Dodds, R. K.; Byren, R. All-Dielectric Subwavelength Metasurface Focusing Lens. *Opt. Express* **2014**, *22* (21), 26212.

(18) Khorasaninejad, M.; Capasso, F. Metalenses: Versatile Multifunctional Photonic Components. *Science* **2017**, *358* (6367), eaam8100.

(19) Lalanne, P.; Chavel, P. Metalenses at Visible Wavelengths: Past, Present, Perspectives. *Laser Photonics Rev.* **2017**, *11* (3), 1600295.

(20) Tseng, M. L.; Hsiao, H. H.; Chu, C. H.; Chen, M. K.; Sun, G.; Liu, A. Q.; Tsai, D. P. Metalenses: Advances and Applications. *Adv. Opt. Mater.* **2018**, *6* (18), 1−16.

(21) Lin, D.; Fan, P.; Hasman, E.; Brongersma, M. L. Dielectric Gradient Metasurface Optical Elements. *Science* **2014**, *345* (6194), 298−302.

(22) Lalanne, P.; Astilean, S.; Chavel, P.; Cambril, E.; Launois, H. Blazed Binary Subwavelength Gratings with Efficiencies Larger than Those of Conventional Échelette Gratings. *Opt. Lett.* **1998**, *23* (14), 1081.

(23) Aieta, F.; Genevet, P.; Kats, M.; Capasso, F. Aberrations of Flat Lenses and Aplanatic Metasurfaces. *Opt. Express* **2013**, *21* (25), 31530.

(24) Chen, W. T.; Zhu, A. Y.; Sanjeev, V.; Khorasaninejad, M.; Shi, Z.; Lee, E.; Capasso, F. A Broadband Achromatic Metalens for Focusing and Imaging in the Visible. *Nat. Nanotechnol.* **2018**, *13* (3), 220−226.

(25) Wang, S.; Wu, P. C.; Su, V. C.; Lai, Y. C.; Hung Chu, C.; Chen, J. W.; Lu, S. H.; Chen, J.; Xu, B.; Kuan, C. H.; Li, T.; Zhu, S.; Tsai, D. P. Broadband Achromatic Optical Metasurface Devices. *Nat. Commun.* **2017**, *8* (1), 1−9.

(26) Shrestha, S.; Overvig, A. C.; Lu, M.; Stein, A.; Yu, N. Broadband Achromatic Dielectric Metalenses. *Light: Sci. Appl.* **2018**, *7* (1), 85 DOI: 10.1038/s41377-018-0078-x.

(27) Zhou, Y.; Kravchenko, I. I.; Wang, H.; Nolen, J. R.; Gu, G.; Valentine, J. Multilayer Noninteracting Dielectric Metasurfaces for Multiwavelength Metaoptics. *Nano Lett.* **2018**, *18* (12), 7529−7537.

(28) Arbabi, A.; Arbabi, E.; Kamali, S. M.; Horie, Y.; Han, S.; Faraon, A. Miniature Optical Planar Camera Based on a Wide-Angle Metasurface Doublet Corrected for Monochromatic Aberrations. *Nat. Commun.* **2016**, *7*, 1−31.

(29) Groever, B.; Chen, W. T.; Capasso, F. Meta-Lens Doublet in the Visible Region. *Nano Lett.* **2017**, *17* (8), 4902−4907.

(30) Engelberg, J.; Zhou, C.; Mazurski, N.; Bar-David, J.; Kristensen, A.; Levy, U. Near-IR Wide Field-of-View Huygens Metalens for Outdoor Imaging Applications. *arXiv: 1901.07331* **2019**.

(31) Shalaginov, M. Y.; An, S.; Yang, F.; Su, P.; Lyzwa, D.; Agarwal, A.; Zhang, H.; Hu, J.; Gu, T. A Single-Layer Panoramic Metalens with > 170 Degree Diffraction-Limited Field of View. *arXiv: 1908.03626* **2019**.

(32) Epstein, A.; Eleftheriades, G. V. Huygens' Metasurfaces via the Equivalence Principle: Design and Applications. *J. Opt. Soc. Am. B* **2016**, *33* (2), A31.

(33) Pfeiffer, C.; Emani, N. K.; Shaltout, A. M.; Boltasseva, A.; Shalaev, V. M.; Grbic, A. Efficient Light Bending with Isotropic Metamaterial Huygens' Surfaces. *Nano Lett.* **2014**, *14* (5), 2491−2497.

(34) Shalaev, M. I.; Sun, J.; Tsukernik, A.; Pandey, A.; Nikolskiy, K.; Litchinitser, N. M. High-Efficiency All-Dielectric Metasurfaces for Ultracompact Beam Manipulation in Transmission Mode. *Nano Lett.* **2015**, *15* (9), 6261−6266.

(35) Zhang, L.; Ding, J.; Zheng, H.; An, S.; Lin, H.; Zheng, B.; Du, Q.; Yin, G.; Michon, J.; Zhang, Y.; Fang, Z.; Shalaginov, M. Y.; Deng, L.; Gu, T.; Zhang, H.; Hu, J. Ultra-Thin High-Efficiency Mid-Infrared Transmissive Huygens Meta-Optics. *Nat. Commun.* **2018**, *9* (1), 1481.

(36) Decker, M.; Staude, I.; Falkner, M.; Dominguez, J.; Neshev, D. N.; Brener, I.; Pertsch, T.; Kivshar, Y. S. High-Efficiency Dielectric Huygens' Surfaces. *Adv. Opt. Mater.* **2015**, *3* (6), 813−820.

(37) Chen, M.; Kim, M.; Wong, A. M. H.; Eleftheriades, G. V. Huygens' Metasurfaces from Microwaves to Optics: A Review. *Nanophotonics* **2018**, *7* (6), 1207−1231.

(38) Yu, Y. F.; Zhu, A. Y.; Paniagua-Domínguez, R.; Fu, Y. H.; Luk'yanchuk, B.; Kuznetsov, A. I. High-Transmission Dielectric Metasurface with 2π Phase Control at Visible Wavelengths. *Laser Photonics Rev.* **2015**, *9* (4), 412−418.

(39) Chong, K. E.; Wang, L.; Staude, I.; James, A. R.; Dominguez, J.; Liu, S.; Subramania, G. S.; Decker, M.; Neshev, D. N.; Brener, I.; Kivshar, Y. S. Efficient Polarization-Insensitive Complex Wavefront Control Using Huygens' Metasurfaces Based on Dielectric Resonant Meta-Atoms. *ACS Photonics* **2016**, *3* (4), 514−519.

(40) Liu, S.; Vaskin, A.; Campione, S.; Wolf, O.; Sinclair, M. B.; Reno, J.; Keeler, G. A.; Staude, I.; Brener, I. Huygens' Metasurfaces Enabled by Magnetic Dipole Resonance Tuning in Split Dielectric Nanoresonators. *Nano Lett.* **2017**, *17* (7), 4297−4303.

(41) Buralli, D. A.; Morris, G. M. Design of a Wide Field Diffractive Landscape Lens. *Appl. Opt.* **1989**, *28* (18), 3950.

(42) Maguid, E.; Yulevich, I.; Veksler, D.; Kleiner, V.; Brongersma, M. L.; Hasman, E. Photonic Spin-Controlled Multifunctional Shared-Aperture Antenna Array. *Science* **2016**, *352* (6290), 1202−1206.

(43) Arbabi, E.; Arbabi, A.; Kamali, S. M.; Horie, Y.; Faraon, A. Multiwavelength Metasurfaces through Spatial Multiplexing. *Sci. Rep.* **2016**, *6*, 1−8.

(44) Khorasaninejad, M.; Chen, W. T.; Devlin, R. C.; Oh, J.; Zhu, A. Y.; Capasso, F. Metalenses at Visible Wavelengths: Diffraction-Limited Focusing and Subwavelength Resolution Imaging. *Science* **2016**, *352* (6290), 1190−1194.

(45) Presutti, F.; Monticone, F. Focusing on Bandwidth: Achromatic Metalens Limits. *Optica* **2020**, *7* (6), 624.

(46) Colburn, S.; Zhan, A.; Majumdar, A. Metasurface Optics for Full-Color Computational Imaging. *Sci. Adv.* **2018**, *4* (2114), 1−7.

(47) Arbabi, A.; Horie, Y.; Bagheri, M.; Faraon, A. Dielectric Metasurfaces for Complete Control of Phase and Polarization with Subwavelength Spatial Resolution and High Transmission. *Nat. Nanotechnol.* **2015**, *10* (11), 937−943.

(48) Kamali, S. M.; Arbabi, A.; Arbabi, E.; Horie, Y.; Faraon, A. Decoupling Optical Function and Geometrical Form Using Conformal Flexible Dielectric Metasurfaces. *Nat. Commun.* **2016**, *7*, 11618.

(49) Hu, T.; Tseng, C.-K.; Fu, Y. H.; Xu, Z.; Dong, Y.; Wang, S.; Lai, K. H.; Bliznetsov, V.; Zhu, S.; Lin, Q.; Gu, Y. Demonstration of Color Display Metasurfaces via Immersion Lithography on a 12-Inch Silicon Wafer. *Opt. Express* **2018**, *26* (15), 19548.

(50) Arbabi, E.; Arbabi, A.; Kamali, S. M.; Horie, Y.; Faraji-Dana, M. S.; Faraon, A. MEMS-Tunable Dielectric Metasurface Lens. *Nat. Commun.* **2018**, *9* (1), 812.

(51) *Paris Panorama*; Wikimedia, 2013. https://commons. wikimedia.org/wiki/File:Paris_panorama_from_Arc_de_Triomphe_ de_l%27Étoile,_10_May_2013.jpg.

(52) Lin, H.; Li, L.; Deng, F.; Ni, C.; Danto, S.; Musgraves, J. D.; Richardson, K.; Hu, J. Demonstration of Mid-Infrared Waveguide Photonic Crystal Cavities. *Opt. Lett.* **2013**, *38* (15), 2779−2782.

(53) Wang, J.; Hu, J.; Sun, X.; Agarwal, A. M.; Kimerling, L. C.; Lim, D. R.; Synowicki, R. A. Structural, Electrical, and Optical Properties of Thermally Evaporated Nanocrystalline PbTe Films. *J. Appl. Phys.* **2008**, *104* (5), 053707.

(54) Wang, J.; Hu, J.; Becla, P.; Agarwal, A. M.; Kimerling, L. C. Room-Temperature Oxygen Sensitization in Highly Textured, Nanocrystalline PbTe Films: A Mechanistic Study. *J. Appl. Phys.* **2011**, *110* (8), 083719.

(55) Born, M.; Wolf, E. quot;*Principles of Optics: Electromagnetic Theory of Propagation, Interference and Diffraction of Light*; Interference and Diffraction of Light, 2000.